

An iterative method for non-uniform illumination correction based on the gray-weighted distance transform of the magnitude spectrum

Abstract

This paper presents a novel filter based method for the suppression of non-uniform illumination without any prior information about the artifact model. The proposed approach iteratively suppresses the frequencies that are responsible for producing the non-uniform illumination in an image. The gray-weighted distance transform (GWDT) has been used in the Fourier domain to automatically find the frequencies responsible for the non-uniform illumination. Moreover, the proposed filtering method is not user dependent and all of the parameters of the filter are automatically generated on the basis of the gray-weighted distance transform of the magnitude of the Fourier transform. Theoretical foundations of the proposed method along with experimental results are reported in this paper. The proposed method has been tested on four different modalities which makes this approach different and unique from most of the existing methods in this field of study. Experimental results demonstrate the superiority of our approach in comparison with some of the existing techniques.

Index Terms

Non-uniform illumination, gray-weighted distance transform (GWDT), center shifted Fourier transform

I. Introduction

Non-uniform illumination is considered as one of the major challenges in the field of medical imaging. It is often caused by the imperfections of the data acquisition device and the properties of the object under study. It is commonly referred to as shading, intensity inhomogeneity or bias field [1]. Non-uniform illumination correction is often considered as a prerequisite to image segmentation [2]. The performance of image matching, retrieval and tracking algorithms are also effected by the presence of the non-uniform illumination [3], [4]. This wide range of applications has lead to the development of a plethora of algorithms. A brief review of the development during the last decade is reported in [1]. In general, these methods can be classified into filtering, surface fitting and histogram thresholding [1].

An image is considered as a product of illumination and reflectance with some noise added by the acquisition device. Mathematically, it can be written as:

$$f(x, y) = i(x, y)r(x, y) + \eta(x, y), \quad (1)$$

where $i(x, y)$ is the amount of the source illumination incident on the scene being viewed, $r(x, y)$ is the amount of illumination reflected by the objects in the scene, and $\eta(x, y)$ is the noise induced by the acquisition device [5]. The value of $i(x, y)$ can vary from zero to infinity and the value of $r(x, y)$ can vary from zero to one, i.e., from absorption to total reflectance. The non-uniform illumination is typically very smooth across the whole image, i.e., it varies slowly and has only very low frequency components [2].

In [6], a surface fitting method was proposed where a bivariate polynomial of degree N was used to estimate the non-uniform illumination in the image. The method is based on the multiplicative image model; it was assumed that the given image is a product of the non-uniform illumination and the true signal with some additive noise. The additive noise was reduced by using a Gaussian filter and the multiplicative model was converted into an additive one by logarithmic transformation. The model parameters were calculated from the gradient of the smoothed image by using a weighted least squares method. An exponential weighting function was used to give small weights to the pixels with large gradient magnitudes and vice versa. The method is computationally expensive, as one needs to solve a system of $2P(N+1)(N+2)/2 - 1$ linear equations to find the $(N+1)(N+2)/2$ parameters, where P is the total

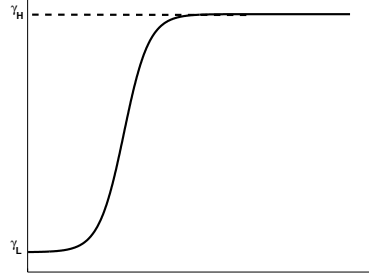


Fig. 1. Homomorphic filter. For explanation on homomorphic filtering, see text. The plot shows the cross section of a circularly symmetric filter.

number of pixels and N is the degree of the polynomial. The performance of the method is dependent on the degree of the polynomial used to estimate the bias field. Furthermore, the method is quite sensitive to the choice of the parameter in the weighting function.

Y. Zheng, et al. [7] proposed a method based on the sparseness property of the gradient probability distribution function. Maximum a posteriori (MAP) estimation with the sparseness prior of the image gradient was used to estimate the non-uniform illumination in natural images. It is based on the assumption that adjacent pixels have the same intensities unless separated by edges [7], which is seldom true for all image modalities. The method works well as long as the image follows the sparseness property of the gradient probability distribution function. This method is also computationally expensive and heavily depends on the parameters of the weighting function. Here, it is worth mentioning that the gradient magnitude must in general be sampled at twice the original sampling rate to avoid aliasing [8], which was not followed in [7]. Doubling the sampling rate will at least double the computational cost of the method proposed in [7].

Homomorphic unsharp masking (HUM) is one of the most common approaches to cope with non-uniform illumination [5], [9]. The main idea is to suppress the low frequency content of the image by multiplying them with a smaller value (γ_L) and increasing the magnitude of the high frequency content by multiplying them with a larger value (γ_H) as shown in Fig. 1. For better performance, HUM requires fine tuning of three parameters, γ_L , γ_H and c , where c controls the transition of the filter. One of the main challenges in using the HUM is to determine the order and the cut-off of the filter. In a qualitative analysis [10], it was reported that HUM-based mean filtering outperforms HUM-based median filtering. It was also concluded that a window size of 65×65 or larger (to apply this method to other images, the window size should be scaled inversely with voxel size to maintain the window size in millimeters) is appropriate. If HUM is applied to an image composed by a gray foreground with dark background, like most medical images, it produces halo artifacts on the boundaries [11]. It is easily visible when a large window is used in HUM. Guillemaud filter [12] was successfully used in [13], [11], [14] to avoid halo artifacts. In [15], the authors proposed an automatic way to select the cut-off frequency for HUM. Later on, the method was generalized to 3D in [11].

In this effort, we propose an iterative method based on the assumption that low frequencies responsible for the non-uniform illumination have higher magnitude than other components. It is intuitive that the non-uniform illumination is observable, when the magnitude of the low frequencies responsible for the degradation is much higher than the rest of the image. Our method is based on the gray-weighted distance transform [16] of the power spectrum of an input image.

The paper is organized as follows. Section 2 will cover the details of the proposed method. Section 3 deals with the experimental set-up used in this paper. Furthermore, Section 4 describes the quantitative and analytical evaluation of the proposed method. Finally, conclusions are presented in the last section.

II. Method

A. Image Fourier Transform

According to the Fourier transform, an image can be expressed as a sum of weighted sinusoids of varying frequencies [17], [18]:

$$F(u, v) = \frac{1}{MN} \sum_{x=0}^{M-1} \sum_{y=0}^{N-1} f(x, y) e^{-2\pi j(\frac{ux}{M} + \frac{vy}{N})} \quad (2)$$

where the $F(u, v)$ is the complex-valued function of the sinusoid passing through the whole image $f(x, y)$ of size $M \times N$. Here, frequency (u, v) is defined in terms of cycles per image. A two-dimensional (2D) sinusoid has two frequencies which represents the frequency of oscillation along the horizontal and vertical spatial dimensions of an image, respectively. A 2D sinusoid is characterised by the frequency (ω) , magnitude $(|F(u, v)|)$, phase $(\angle F(u, v))$ and direction of the fastest oscillation (\vec{n}) , whereas a one-dimensional (1D) sinusoid is represented by its frequency, magnitude and phase. Mathematically, the four characteristics of a 2D Fourier transform can be expressed as:

$$\begin{aligned} \omega &= \sqrt{u^2 + v^2}, \\ \vec{n} &= \tan^{-1}\left(\frac{v}{u}\right), \\ |F(u, v)| &= \sqrt{\Re(F(u, v))^2 + \Im(F(u, v))^2}, \\ \angle F(u, v) &= \tan^{-1}\left(\frac{\Im(F(u, v))}{\Re(F(u, v))}\right), \end{aligned} \quad (3)$$

Generally, the illumination component of an image is characterised by slow spatial variations, while the reflectance component tends to vary abruptly, particularly at the junctions of dissimilar objects [5]. In the Fourier transform, the illumination is modelled by the low frequency sinusoids and the reflectance is characterised by the high frequency sinusoids. In general, the magnitude of the Fourier transform decreases rapidly as one moves away from the origin, i.e., from lowest to highest frequency. Essentially, one can incur that the magnitudes of the low frequencies are higher than their counterparts. So, one can interpret the addition of non-uniform illumination to an image as a change in the magnitude of the low frequencies. The phase of these low frequencies will also be altered, but this is beyond the scope of this paper.

B. Image Restoration using Fourier Transform

The main task of the non-uniform illumination correction is to adjust the magnitudes of those low frequencies that are affected by the addition of non-uniform illumination. Now, a simple question arises: how and where to find those frequencies in the Fourier transform? Theoretically, the question is complex to answer. Usually, this is solved empirically with user interaction where the user selects the appropriate parameters of the filter which suppresses the responsible frequencies. Normally, circular filters are used due to the lack of information about the location of the frequencies that are responsible for the degradation of an image. Another reason for using circular filters is the ease in their design [11]. The circular filter not only suppresses the frequencies which produces the non-uniform illumination but also removes the additional frequency content of the image which often results in high-pass look of the resulting image. So, it is desirable to only suppress the frequencies that are responsible for the non-uniform illumination and to have very low effect on rest of the frequency content of the image. During the literature review for this study, we have found that most of the methods used for the suppression of the non-uniform illumination requires user interaction where the parameters need to be finely tuned by the user based on his/her visual inspection. In this paper, we propose a filter-based approach for the suppression of the non-uniform illumination where the filter is automatically generated based on the frequency content of the given input image.

C. The Proposed Approach

An automatic strategy has been proposed which constructs a low-pass filter based on the assumption that the addition of the non-uniform illumination will amplify the magnitude of the low frequencies. So, we can expect a relatively higher magnitude for those low frequencies as compared to their neighbours in the Fourier transform. Our method produces a filter that is based on the frequency content of an image. This also means that the shape of the filter (regular or irregular) depends on the distribution of frequencies responsible for non-uniform illumination. In most of the situations, the shape of the filter turns out to be irregular. To the best of our knowledge, this prior information has never been used in filter design nor it has been considered by the user while choosing the cut-off of the filter. Another crucial issue is how much the magnitude of the low-frequencies responsible for non-uniform illumination should be suppressed. Should it be suppressed completely? In HUM, this is controlled by (γ_L) which is also selected by the user on the basis of the visual inspection. We have proposed an iterative procedure which automatically selects the amount of magnitude of the low frequencies responsible for non-uniform illumination that needs to be attenuated. This is extremely important as complete suppression of these low frequencies can produce further non-uniformity in the image. In other words, retaining a certain amount of magnitude of these low frequencies is necessary to produce the uniformly illuminated image. The proposed method is summarized below.

Algorithm 1 Irregular Low-pass Filter based on Gray-Weighted Distance Transform (GWDT) of Power Spectrum

```

1: im = read_image(input_image);
2: IM = fftshift(fft2(im)); // Compute the centered shifted Fourier transform (CSFT)
3: j = 0; // initialization
4: similarity[j] = 1; // initialization
5: repeat
6:   j = j+1;
7:   IM_magnitude = abs(IM); // Magnitude calculation
8:   Distance = GWDT(IM_magnitude); // Compute the distance map using GWDT
9:   for i = 1, ..., n do
10:     Dist = (Distance ≤ i) × IM; // where (Distance ≤ i) is a binary mask of the same size as IM.
11:     POWER(i) =  $\frac{\sum(\text{abs}(Dist)^2)}{\sum(\text{abs}(IM)^2)}$  × 100; // Calculating the percentage of the power spectrum
12:   end for
13:   Select a threshold value (thresh);
14:   Mask = Distance ≤ thresh;
15:   Convolution of the Mask with Gaussian and name it as Low_Pass; // Mask smoothing
16:   High_Pass = max(Low_Pass) - Low_Pass;
17:   ADJUSTED = High_Pass × IM; // High pass filtering in the Fourier domain
18:   IM_magnitude = ADJUSTED;
19:   adjusted = real(ifft2(ifftshift(ADJUSTED)));
20:   similarity[j] = correlation(adjusted,im);
21: until 0 ≤ (similarity[j-1]-similarity[j]) ≤ ε

```

1) Proposed Method: The proposed method starts by calculating the magnitude of the Fourier transform of the given input image as shown in Fig. 2(b). This magnitude image becomes an input to the gray-weighted distance transform (GWDT) [16]. Distances computed using GWDT, not only incorporates the spatial closeness but also the similarity between the gray-levels of the pixels (in our case, it is the magnitudes of the frequencies). The cost $c_i = c(x_i, x_{i+1})$ of the gray-weighted distance (GWD) is defined as the cost of travelling from a pixel x_i to an adjacent pixel x_{i+1} on a geodesic mask. The GWD $d(p, q)$

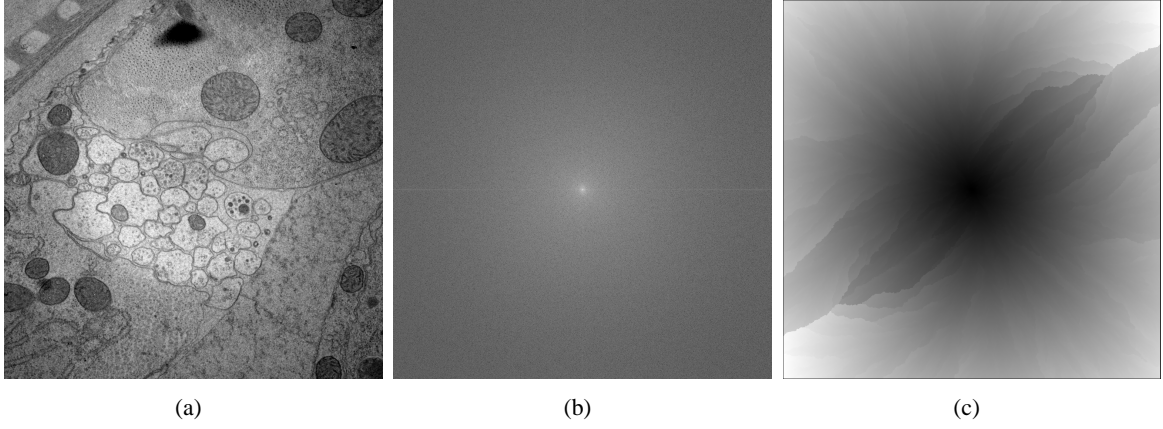


Fig. 2. a) Original TEM image of a rabbit retina. b) Magnitude of the CSFT of 2(a), c) Result after applying GWDT on 2(b).

is defined as the path of the minimum cost from p to q . It can be written as:

$$d(p, q) = \left\{ \min_{P \in \mathcal{C}_{pq}} (\mathcal{C}(P)) \quad | \quad \mathcal{C}(P) = \sum_{i=1}^{l-1} c_i \right\}, \quad (4)$$

where c is computed as:

$$c(x_i, x_{i+1}) = |f(x_i) - f(x_{i+1})| \cdot \|x_i - x_{i+1}\|, \quad (5)$$

where $f(x_{i+1})$ is a gray-level value at pixel x_{i+1} .

Readers interested in deep understanding of GWDT are advised to refer to [16], [19]. In our proposed approach, the DC component of the magnitude of the *centered shifted Fourier transform* (CSFT) serves as the only seed point for the GWDT. Fig. 2(c) shows the result of applying GWDT on the magnitude (*IM_magnitude*) of the CSFT. As we are interested in suppressing the magnitude of those low frequency contents that are relatively higher in magnitude and spatially close to the DC component, GWDT is one of the methods that can be used to fulfil both constraints. Those low frequencies will acquire relatively small values in the GWDT as shown in Fig. 2(c). Here, the lowest value is zero, i.e., the distance from the seed to itself. The range of the values from low to high shows the GWD from the seed.

The next step of our proposed method is to compute the percentage of the power spectrum depending on the GWD. This distance shows the change of frequencies from the DC component in each direction independently, which helps to find the irregular distribution of frequencies responsible for the non-uniform illumination. It is followed by finding the locations of all the low frequencies which are responsible for the non-uniform illumination. To accomplish this, let $M : GWDT \rightarrow F_M$, $x_0 \in GWDT$ and $B(x_0, r)$ is a ball with the centre in x_0 (location of the seed) and radius r , i.e.,

$$B(x_0, r) = \{v \mid d(p, q) < r\}. \quad (6)$$

where v defines the location of a pixel contained within a radius r . Then the set of low frequencies within radius r is defined as:

$$K(x_0, r) = \{M(x) \mid x \in B(x_0, r)\}. \quad (7)$$

It is followed by computing the percentage of the power spectrum ($POWER(r)$) as shown in Fig. 3. Mathematically, it can be written as:

$$POWER(r) = \frac{\Omega(K(x_0, r))}{\Omega(F_M)} \times 100; \quad (8)$$

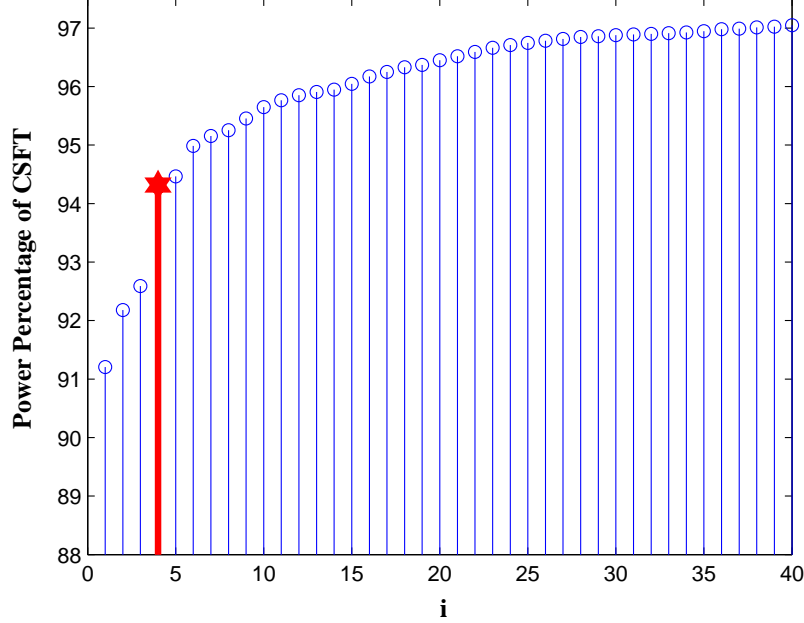


Fig. 3. Power percentage of the CSFT for a ball of radius i .

where the power spectrum of $F(u, v)$ is computed by:

$$\Omega = \sum_{u=0}^{M-1} \sum_{v=0}^{N-1} |F_M(u, v)|^2. \quad (9)$$

The value of r after which the power percentage of *IM_magnitude* for the ball $B(x_0, r)$ stops changing, i.e., becomes almost flat will serve as the threshold (*thresh*). This threshold corresponds to the ball outside which the magnitude in *IM_magnitude* drops abruptly. Essentially, this means that all the low frequencies contained within this ball have got relatively much higher magnitude than the frequencies outside the ball. This ball can take on any shape depending on the magnitude of the frequencies relative to the DC component. This is why a filter based on a ball often turns out to have an irregular shape. According to our observation this threshold is usually between 3 and 5. This threshold value will help us to find an ideal low-pass filter which will correspond to the frequencies responsible for the non-uniform illumination as shown in Fig. 4(a) and Fig. 4(b). It is also important to mention that this threshold is selected in the first iteration and will remain same during rest of the iterations. This is mainly because the frequencies responsible for non-uniform illumination were found in the first iteration and in the later iterations, the magnitude of *only* those frequencies were attenuated gradually. To attenuate those frequencies, an ideal low-pass filter is designed as:

$$F_{low} = \begin{cases} 1 & \text{if } F_{low} \in K(x_0, \text{thresh}) \\ 0 & \text{if } F_{low} \in \overline{K(x_0, \text{thresh})}. \end{cases} \quad (10)$$

To avoid the ringing artifacts produced by an ideal filter, we have smoothed our filter with a Gaussian of $\sigma = 1$ as shown in Fig. 4(c). Now, to stop these frequencies, we will use a *High_Pass* filter as shown in Fig. 4(d), which is produced in step 16 of Algorithm 1. The next step of our proposed approach is to filter the given image by using the *High_Pass* filter and take the resulting image (*adjusted*) back to the spatial domain. The whole process is repeated until the difference between the similarity (as computed in step 20 of Algorithm 1) is less than ϵ . Usually ϵ is set to 0.05, however any value less than 0.1 works

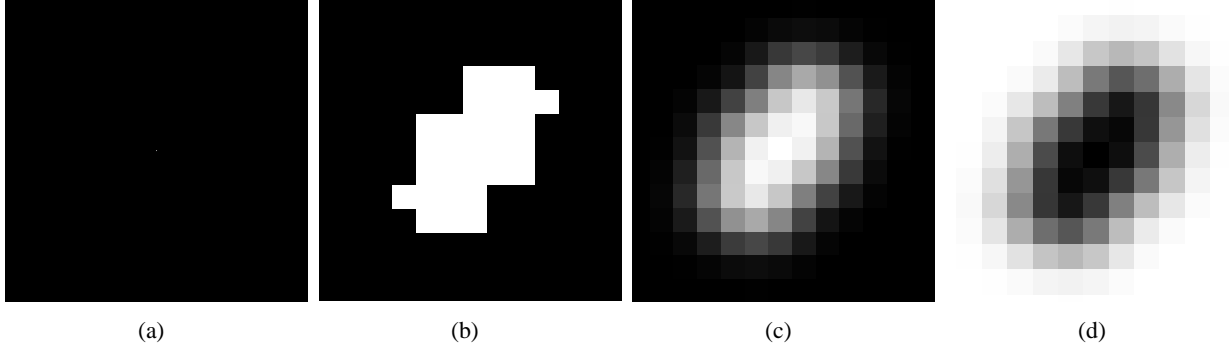


Fig. 4. a) Ideal low-pass filter. b) Zoomed version of the filter in 4(a). c) Smoothed version of the filter in 4(b). d) High-pass filter.

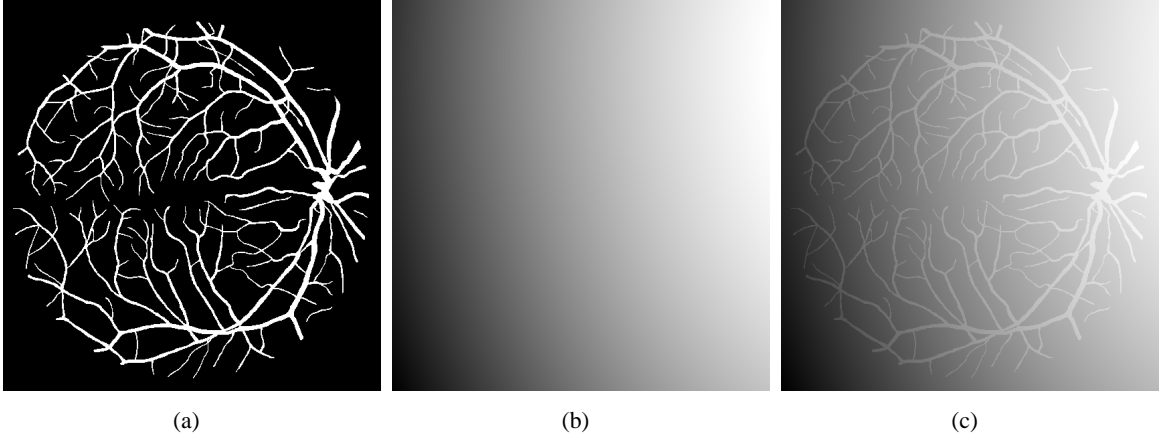


Fig. 5. a) Binary image $B(x, y)$ from the DRIVE database [20]. b) Non-uniform illumination pattern $I_n(x, y)$. c) Non-uniformly illuminated image $P(x, y)$ produced by adding the non-uniform illumination pattern of 5(b) to the binary image.

fine for the applications that we have tested. In each iteration, the filter will try to suppress the low frequencies gradually from one iteration to the next. Empirically, we have noticed that usually the method takes between 3 to 5 iterations to converge.

III. Experimental Setups

In the experimental evaluation of our proposed method, we have used five different types of test images:

- 1) Binary retinal images for setup 1
- 2) Synthetic images (SI) for setup 2
- 3) Transmission Electron Microscopic (TEM) images for setup 3
- 4) Fundus camera (FC) images for setup 4
- 5) Functional Magnetic Resonance Imaging (fMRI)

A. Experimental Setup 1

In the first experiment, we have used 40 binary images from the digital retinal images for vessel extraction (DRIVE) database [20]. Here, a binary image $B(x, y)$ represents the pure reflectance which essentially means that illumination is constant throughout the image as shown in Fig. 5(a). To synthesize the non-uniformly illuminated image $I_n(x, y)$, the first step is to generate an image $R(x, y)$ having values randomly drawn from a standard normal distribution $\mathcal{N}(0, 1)$. It is convolved with a Gaussian low-pass filter G ,

$$P(x, y) = R(x, y) * G_{\mu, \sigma}, \quad (11)$$

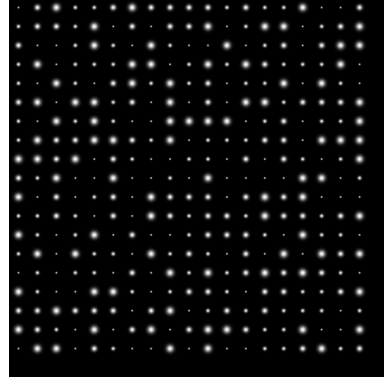


Fig. 6. Synthetic image $S_g(x, y)$, created by using Gaussians of varying sigmas.

where $P(x, y)$ is the synthetic non-uniform illumination pattern and $G(x, y) \sim \mathcal{N}(0, 75)$. Finally, a non-uniformly illuminated synthetic image $I_n(x, y)$ is created by:

$$I_n(x, y) = B(x, y) + P(x, y) \quad (12)$$

One such example is shown in Fig. 5(c), where the synthetic non-uniform illumination pattern $P(x, y)$ as shown in Fig. 5(b), is added to the binary image $B(x, y)$. For simplicity, we are considering the additive image model in Eq. 12 as one can easily transform a multiplicative model into additive by using the logarithmic transform.

B. Experimental Setup 2

In the second experiment, we have created synthetic images $S_g(x, y)$ by using Gaussian of varying sigmas. All these Gaussians were placed randomly in a digital grid with their centers apart from each other by $6 \times \sigma_{max}$, where σ_{max} is the maximum variance of the Gaussians. For each image, four Gaussians of different sigmas were used and they were placed randomly to form an image. One such synthetic image is shown in Fig. 6. Once a synthetic image has been created, different kinds of non-uniform illumination patterns were created by:

$$P(x, y) = A \sin(2\pi(\frac{ux}{M} + \frac{vy}{N})) \quad (13)$$

where A is the amplitude, u is the horizontal frequency, v is the vertical frequency, M is the total number of rows of an image and N is the total number of columns of an image. Different values of u and v were picked randomly between $(0, 0.7]$ for creating sine waves of different frequencies as it resembles the non-uniform illumination pattern produced by different imaging modalities. Finally, the non-uniformly illuminated image $I_n(x, y)$ is created by:

$$I_n(x, y) = S_g(x, y) + P(x, y) \quad (14)$$

A polynomial surface of degree two and three has also been used for the creation of the non-uniform illumination pattern. A third degree polynomial has the following equation:

$$P(x, y; a) = a_1x^3 + a_2y^3 + a_3 \quad (15)$$

where $a = a_1, a_2, a_3$ is the parameter vector that defines the surface. Finally, the non-uniform illuminated image is created by using Eq. 14. Fig. 7 illustrates a few examples of our 400 synthetic images.

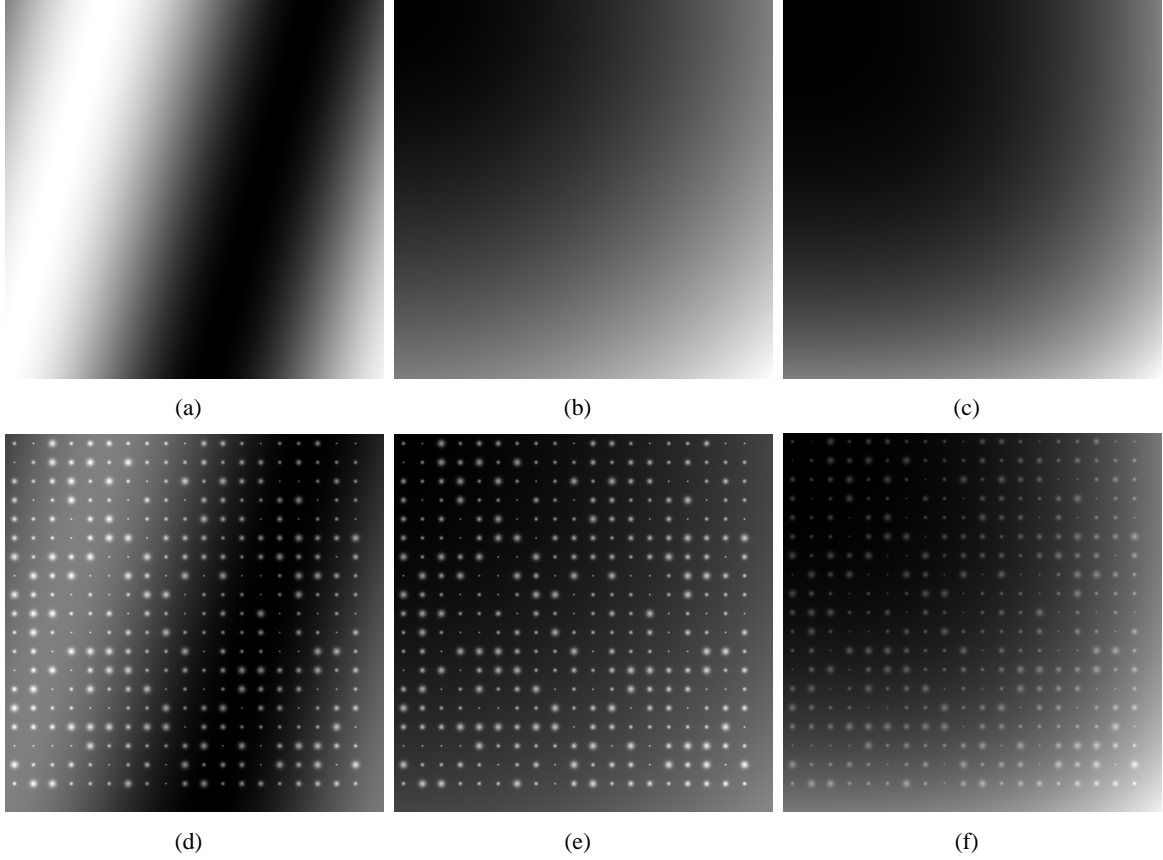


Fig. 7. a) Non-uniform illumination pattern created by using Eq. 13. b) Non-uniformly illumination pattern created by a second order polynomial. c) Non-uniformly illumination pattern created by using Eq. 15. d) Non-uniformly illuminated image created by adding 7(a) with Fig. 6. e) Non-uniform illuminated image created by adding 7(b) with Fig. 6. f) Non-uniformly illuminated image created by adding 7(c) with Fig. 6.

C. Experimental Setup 3

In the third experiment, we have used the transmission electron microscopy (TEM) images of rabbit retina as used in [6]. As TEM provides high-resolution images at nano-meter scale, it becomes rather impractical to use surface-fitting methods due to numerical issues. TEM images often suffer from variations in brightness due to electron imaging defects (non-uniform support films) and specimen staining [6]. Presence of such non-uniformities implies a need for image restoration prior to further image analysis. Hence, they are suitable candidates for our algorithm. One such image is shown in Fig. 8(a), where the non-uniform illumination is evident in the center of the image.

D. Experimental Setup 4

A confocal scanning laser ophthalmoscope is widely used to access the health of the retina. Retinal images often suffer from non-uniform illumination [22] which in return can effect the registration and segmentation process. This also makes the retinal image an ideal candidate to test our algorithm. We have used VICAVR [21], which is a public database. It contains 233 images of 139 individuals. All the images are taken with TopCon non-mydiatic camera NW-100 with a resolution of 768×584 pixels. A few examples from the VICAVR database are shown in Fig. 8(b) and Fig. 8(c).

E. Experimental Setup 5

The literature shows that many of the filtering methods for non-uniform illumination correction are tested on MR images [1]. To have a fair comparison, we have opted to evaluate our method on 3D MR

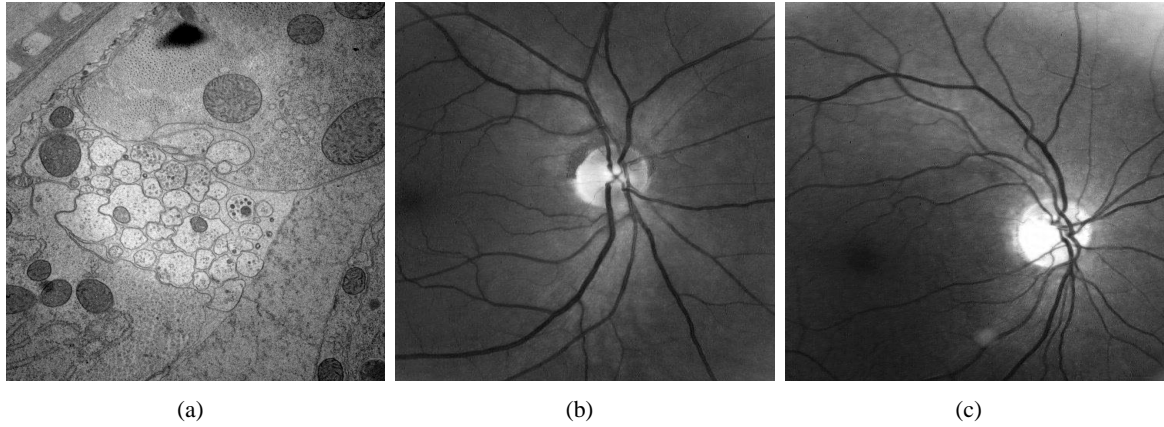


Fig. 8. Images from different modalities. a) TEM image suffering from non-uniform illumination. b), c) Original images from the VICAVR database [21].

volumes obtained from the BrainWeb Simulated Brain Database [23]. This database provides both, the non-uniformly illuminated images as well as the ground truth. In total, we have used, 9 MR brain volumes. The simulated data sets are obtained with the following settings: T1, T2 and PD modalities, slice thickness of 1 mm, 0%, 3% and 7% noise levels, and 40%, 70% and 90% intensity non-uniformity levels. We use the same settings as mentioned in [7] to have a fair comparison of our method. Fig. 9, 10, 11 show a few slices from the test volumes.

IV. Results and Discussion

A. Results of Setup 1

This section will present the evaluation of each experimental setup. In the first experimental setup, a synthetic non-uniform pattern P as introduced in Section III-A was added to a binary image B to produce a non-uniformly illuminated image I_n . One way to evaluate our method in such a situation would be to recover B from I_n . To accomplish this task, we run our method on I_n , which resulted in an image R . Then Otsu's thresholding was applied afterwards on R to convert it into a binary image B_R [24]. A logical “*and*” operation was performed between B and B_R to form a new image BW . Then the ratio between the number of white pixels in BW with number of white pixels in B_R were computed. Fig. 12(a) shows the result of applying Otsu's method when all the 400 test images were preprocessed with our algorithm. We added a random pattern (as described in Section III-A) to each of the 40 binary images. This process was repeated 10 times to produce a test set of 400 images. Our method was able to recover more than 98% of the pixels in all the 400 test cases. Fig. 12(b) shows that the direct application of Otsu's thresholding, on average recovers only 22% of the white pixels.

Moreover, we have used the sinusoidal pattern explained in Section III-B to produce the non-uniformly illuminated images and then used the same evaluation criteria as mentioned earlier in this Section. The result of applying Otsu's thresholding after preprocessing by our proposed method are shown in Fig. 12(c). The result shows that we have recovered 100% pixels in all the 400 test images, while direct application of Otsu's method recovers less than 25% pixels as shown in Fig. 12(d). Here, it is trivial to find the edges in our binary test images, but to find the internal areas of the vessels is a bit tricky. However, our algorithm is able to find the whole structure very efficiently as it was able to exactly locate the low frequency content which was responsible for the non-uniformity in the image.

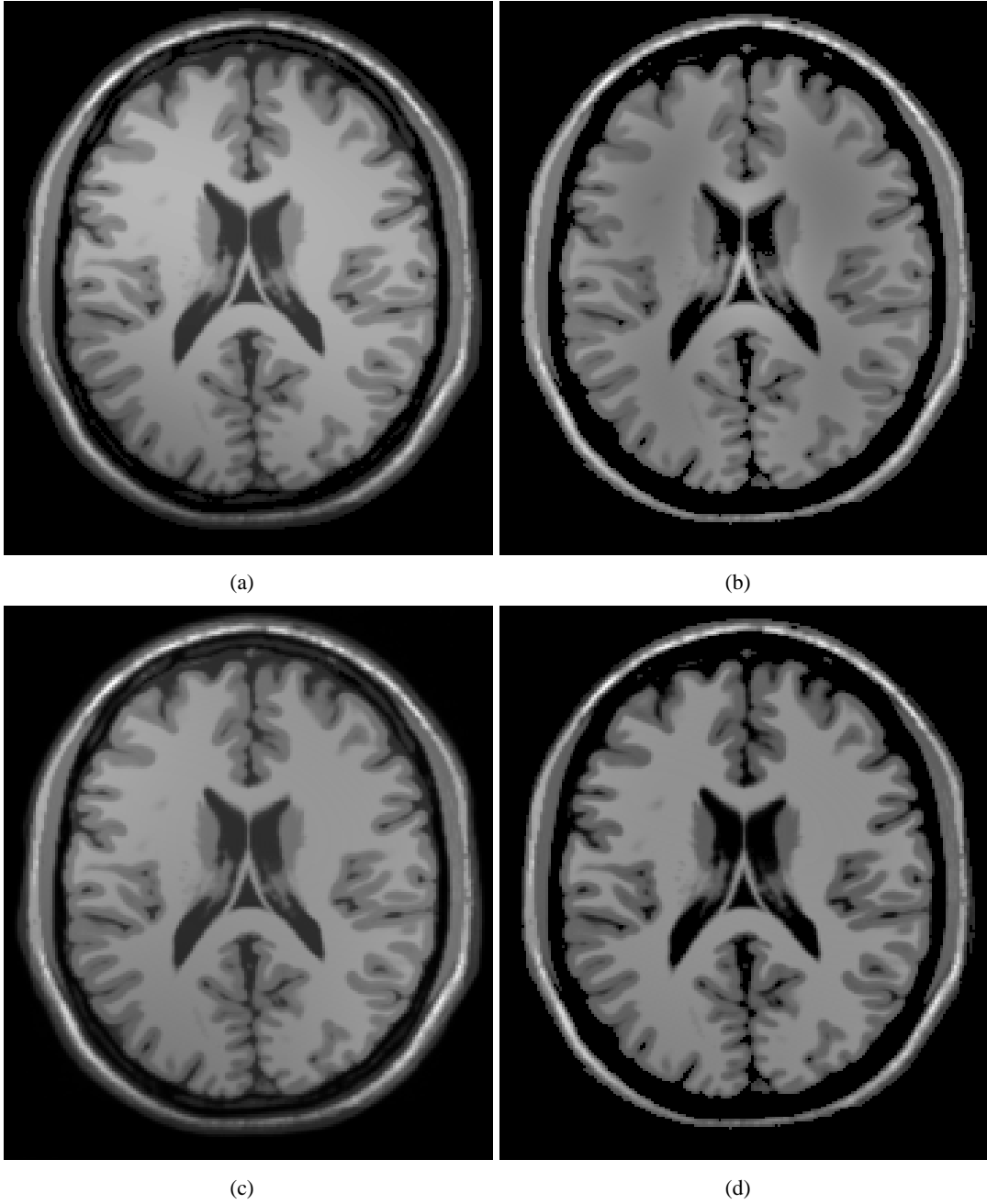


Fig. 9. a) Original image from the brainweb database [23]. b) Result after applying the method proposed in [11]. c) Result after applying the method proposed in [7]. d) Result after applying our method.

B. Results of Setup 2

To evaluate the experimental setup 2, polynomials of degree three were used to show that our proposed algorithm do not produce any artifacts while removing or reducing the non-uniform illumination. To support our hypothesis, we have used cross-correlation as a measure to show the similarity between the original image B and the image B_R produced by our algorithm. Fig. 13 shows the cross-correlation value between B and the non-uniformly illuminated image I_n . Once again 400 test images were produced by using a polynomial having a maximum value of 1500. One such example is shown in Fig. 14(c) while Fig. 14(d) shows the result of our algorithm. This was performed intentionally so that the non-uniformity should corrupt the test image severely. The results of our proposed algorithm under these conditions are shown in Fig. 13(a), while Fig. 13(b) shows the result of taking direct cross-correlation between the

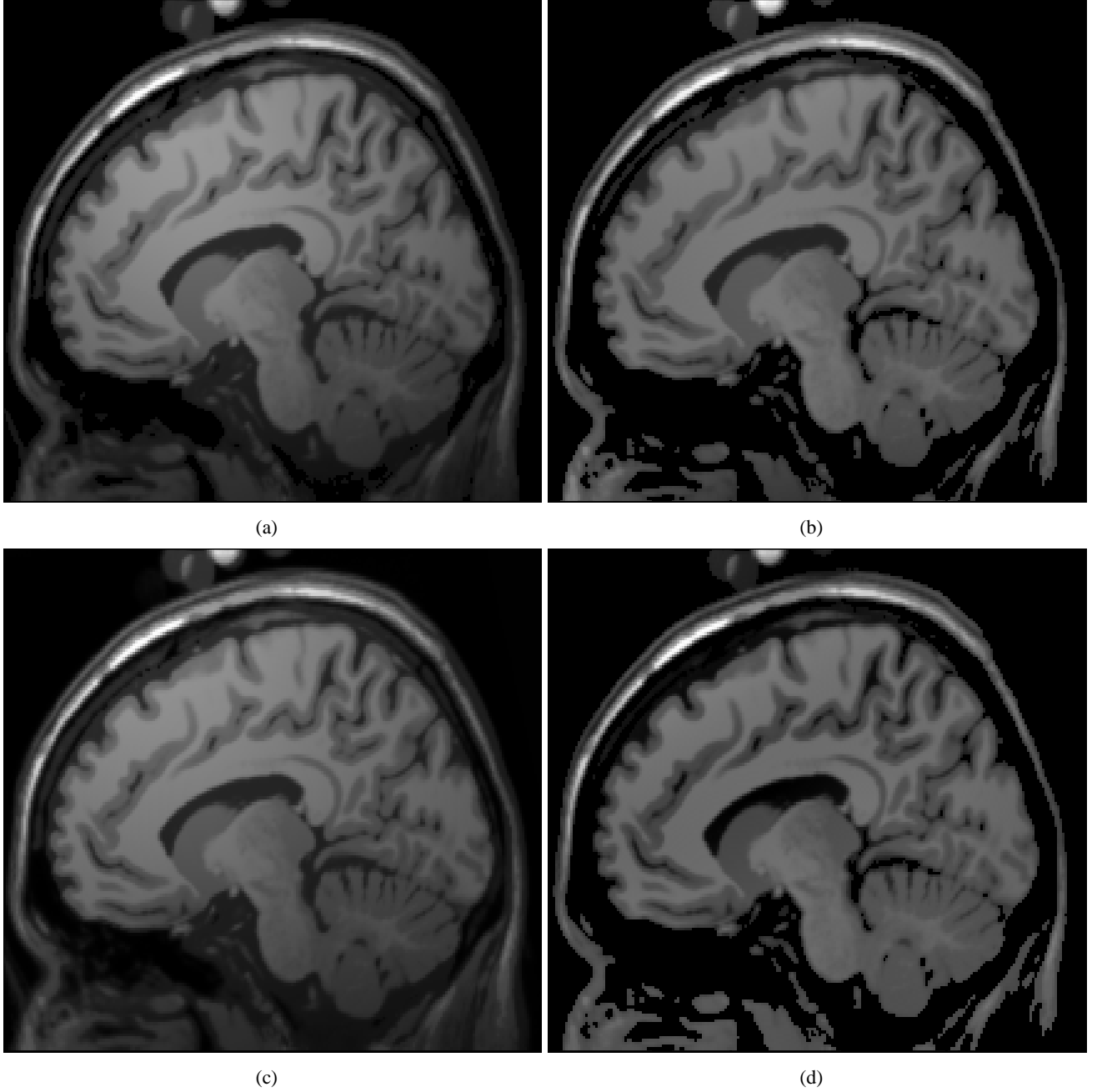


Fig. 10. a) Original image from the brainweb database [23]. b) Result after applying the method proposed in [11]. c) Result after applying the method proposed in [7]. d) Result after applying our method.

original image and the non-uniformly illuminated image. The severity of the non-uniformity is obvious from the horizontal axis of Fig. 13(b) where the maximum cross-correlation value is less than 0.1.

It is obvious that our method is able to recover most of the image content in all presented situations. The same experiment was performed with the non-uniformity produced by sinusoids as we did with the polynomials. The cross-correlation of B with I_n and B with B_R was calculated to prove our hypothesis that our proposed method do not produce any artifacts while removing the non-uniform illumination pattern. Fig. 15 shows the result in histogram format with the same axis as used in Fig. 12. It is worth mentioning that the amplitude of the sinusoid was increased to 800 for testing the robustness of our method.

Fig. 15(a) shows the cross correlation of the original image with the image produced by our algorithm, while Fig. 15(b) shows the result of taking cross correlation between the non-uniformly illuminated image

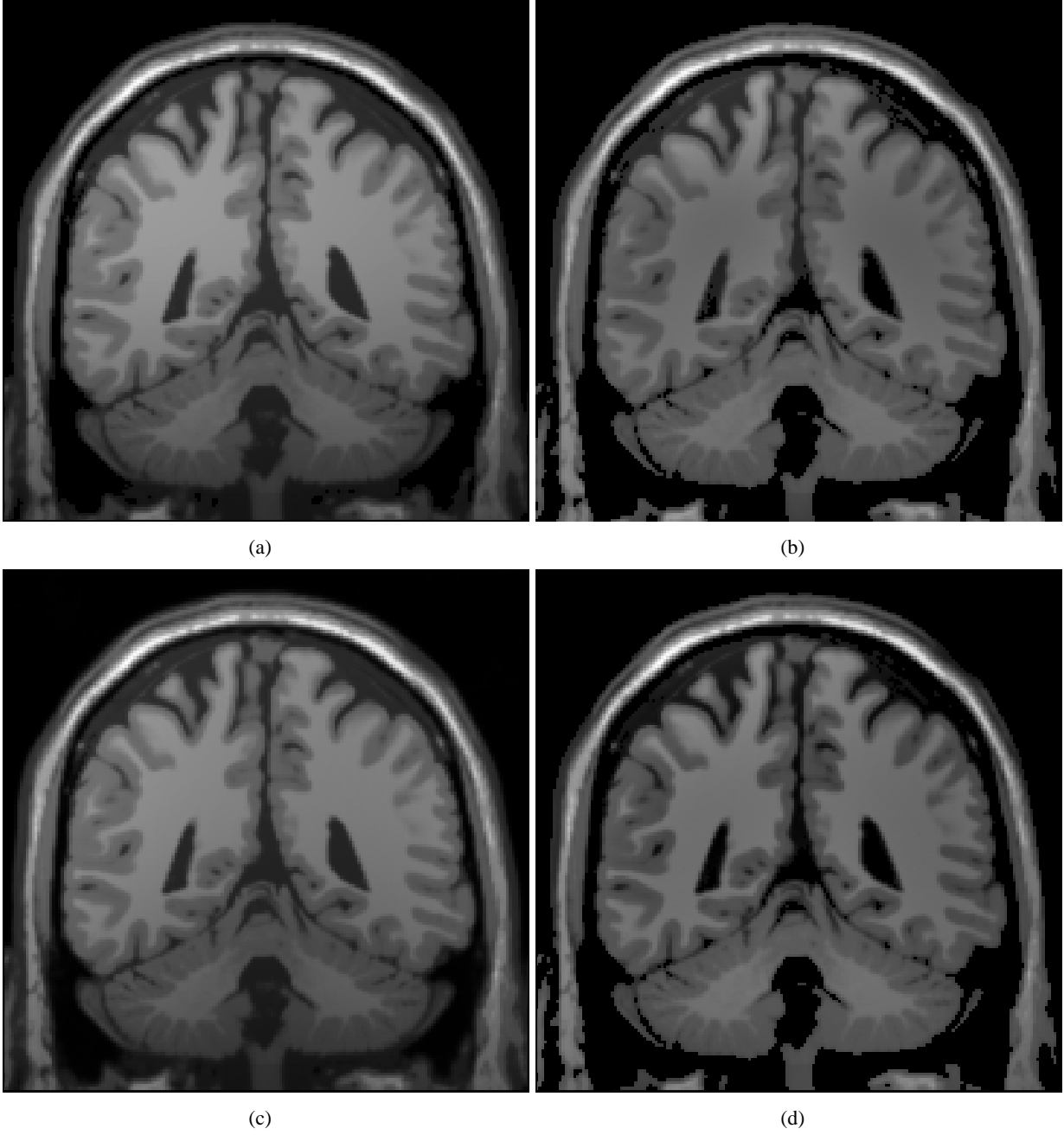


Fig. 11. a) Original image from the brainweb database [23]. b) Result after applying the method proposed in [11]. c) Result after applying the method proposed in [7]. d) Result after applying our method.

and the original image. Fig. 16 shows the result of our proposed method on a test image corrupted with sinusoidal waves.

C. Results of Setup 3-5

The TEM images in experimental setup 3 were compared visually due to lack of ground truth. To have a proper evaluation, we compared our result with results from [14], the surface fitting algorithm given in [6], and the method based on the sparseness property of the gradient probability distribution function [7]. Visual inspection of Fig. 17 clearly shows the effectiveness of our algorithm as compared to other methods.

We use the same procedure to evaluate the experimental setup 4 for the whole database. Fig. 18 shows

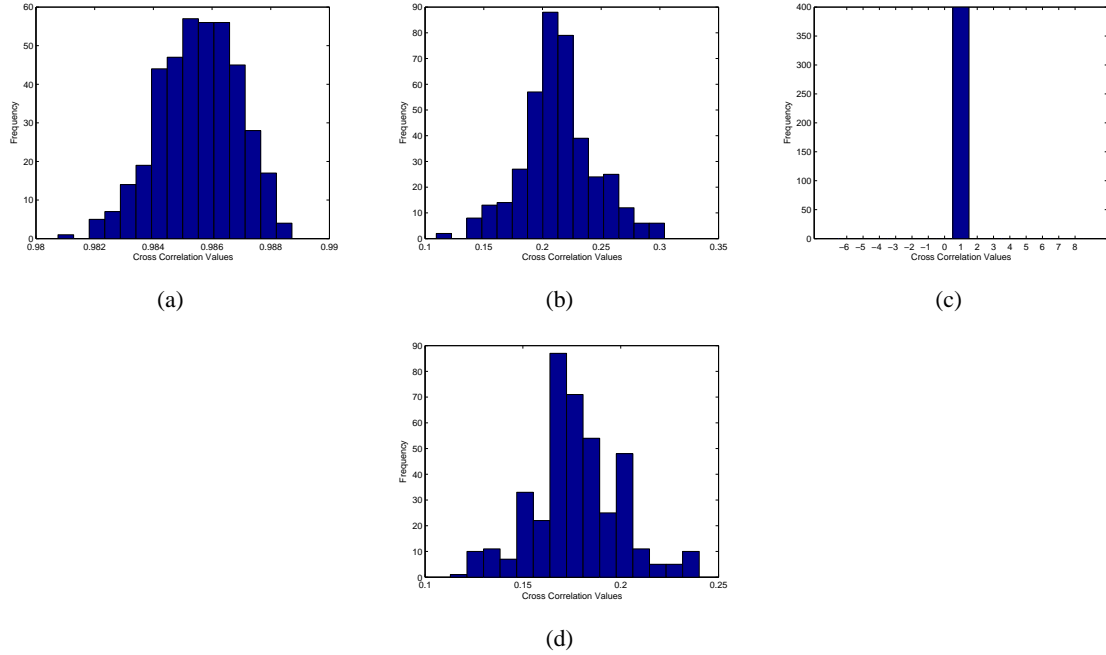


Fig. 12. Percentage histograms. Here, the horizontal axis represents the percentage of correctly classified white pixels, while the vertical axis represents the number of test images. a) Histogram after application of our method. The histogram shows that our method was able to recover 98.5% of the pixels. b) Results of applying direct cross-correlation between the original image and the non-uniformly illuminated image. The histogram shows that one can correctly recover 21% of the pixels. c) Result of our algorithm when a sinusoidal wave was added as a non-uniform pattern. Here, our method was able to recover 100% of the pixels. d) Results of applying direct cross-correlation between the original image and the non-uniformly illuminated image created using the sinusoidal wave. On average, one can only recover 18% pixels in an image.

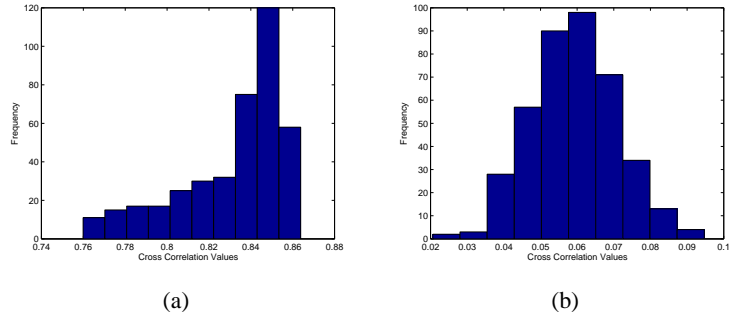


Fig. 13. Histograms, where the horizontal axis represents the cross-correlation value between two images, while the vertical axis represent the number of test images. a) Cross-correlation of images produced by our method and ground truth. Here, the images were corrupted by third degree polynomials. The histogram is centered around 0.84. This clearly shows that our results are quite similar to the ground truth. b) Cross-correlation between the ground truth and non-uniformly illuminated images produced using third degree polynomials. The histogram is centered around 0.06.

the result of applying our algorithm on some of the images from VICAVR [21]. The results obtained here are also quite promising. We followed the same lines to evaluate experimental setup 5 as we did in experimental setups 3 and 4. Moreover, we have used normalized convolution as proposed in [12] to avoid the halo artifacts. Fig. 9, 10, 11 present a comparison of the proposed method with different methods.

For better evaluation of the experimental setups 3, 4 and 5, we have followed the subjective evaluation of the humans that is reported as the most appropriate criteria for the assessment of the image quality [5]. The subjective evaluations can be done by using absolute rating scale or by means of side-by-side comparisons of the original image and the resulting image. In our subjective evaluation, we have followed the side-by-side scale that ranges from -3 to 3 where -3 corresponds to the ***much worse*** and 3 corresponds to ***much better*** image quality. The complete side-by-side scale used in this paper is given in Table I. All

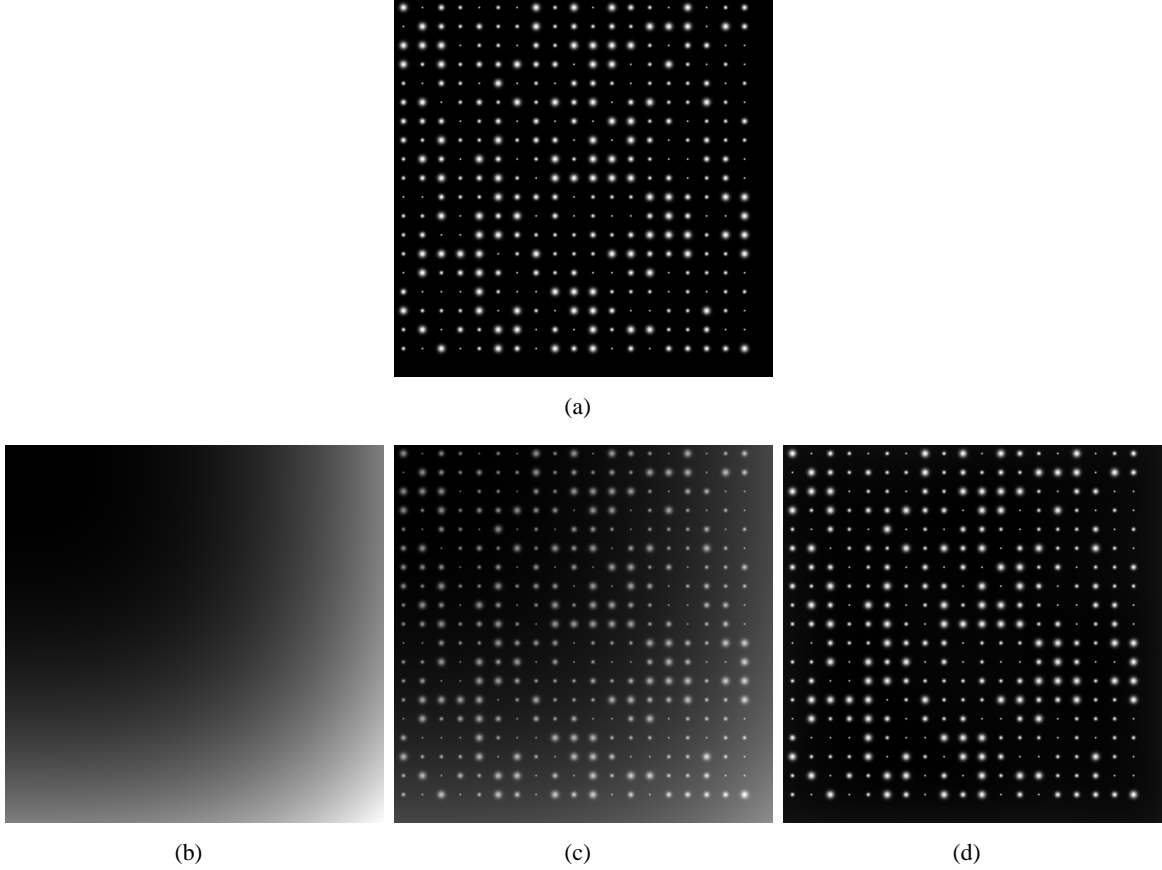


Fig. 14. a) Original image. b) Non-uniform illumination pattern created by a third degree polynomial. c) Non-uniform illuminated image. d) Adjusted image after 5th iteration.

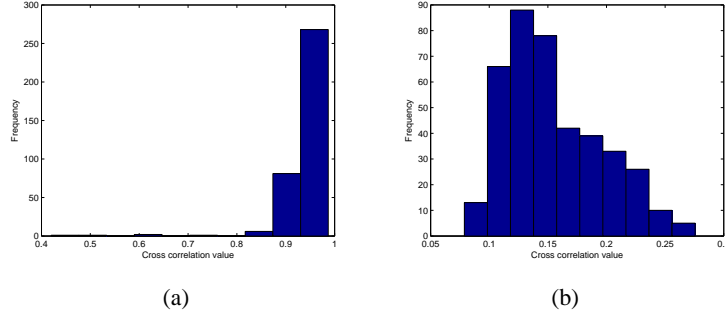


Fig. 15. Histogram images. a) Cross-correlation of images produced by our method and the ground truth. Here, the images were corrupted using sinusoids. The histogram is centered around 0.95 which clearly shows the ability of our method to restore the original image. b) Cross-correlation between the ground truth and non-uniformly illuminated images produced using sinusoids. Here, the mean value is around 0.17.

TABLE I
SIDE-BY-SIDE SCALE FOR SUBJECTIVE EVALUATION

Value	Rating	Description
-3	Much worse	An image of extremely bad quality
-2	Worse	An image of bad quality
-1	Slightly worse	An image of slightly worse quality
0	Same	Same as the original image
1	Slightly better	An image slightly better
2	Better	An image of high quality
3	Much better	An image of extremely high quality

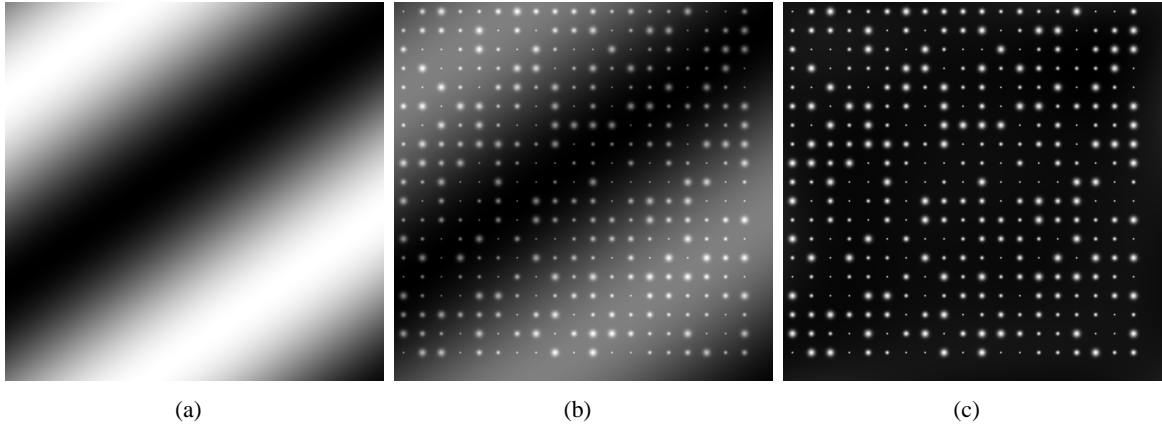


Fig. 16. a) Non-uniform illumination pattern created by a sinusoidal wave. b) Non-uniform illuminated image by adding 16(a) and Fig. 6. c) Corrected image at 5th iteration.

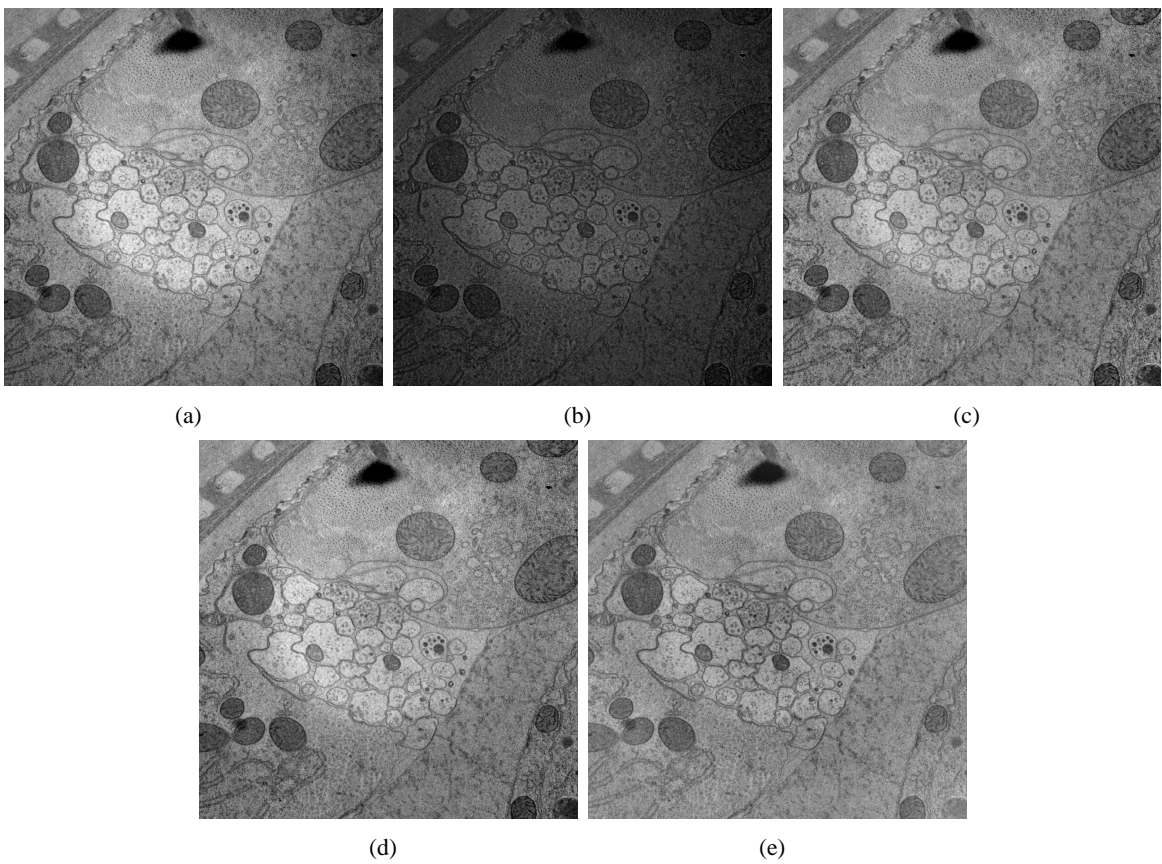


Fig. 17. a) Original image suffering from non-uniform illumination. b) Result of applying homomorphic filtering. c) Result of applying the method described in [6]. d) Result after applying the method mentioned in [7]. e) Result produced by the proposed method.

of the results were displayed on the monitor screen and a small group of students were asked to do the evaluation. In total 18 students participated in this evaluation process who marked the images according to their visual judgement of the images. To make the evaluation process fair, the results were shown to the students without mentioning the results of the proposed method and the results obtained by applying different methods. Fig. 19 show the histograms of the evaluation for the databases used in this paper for experimental setup 3, 4 and 5.

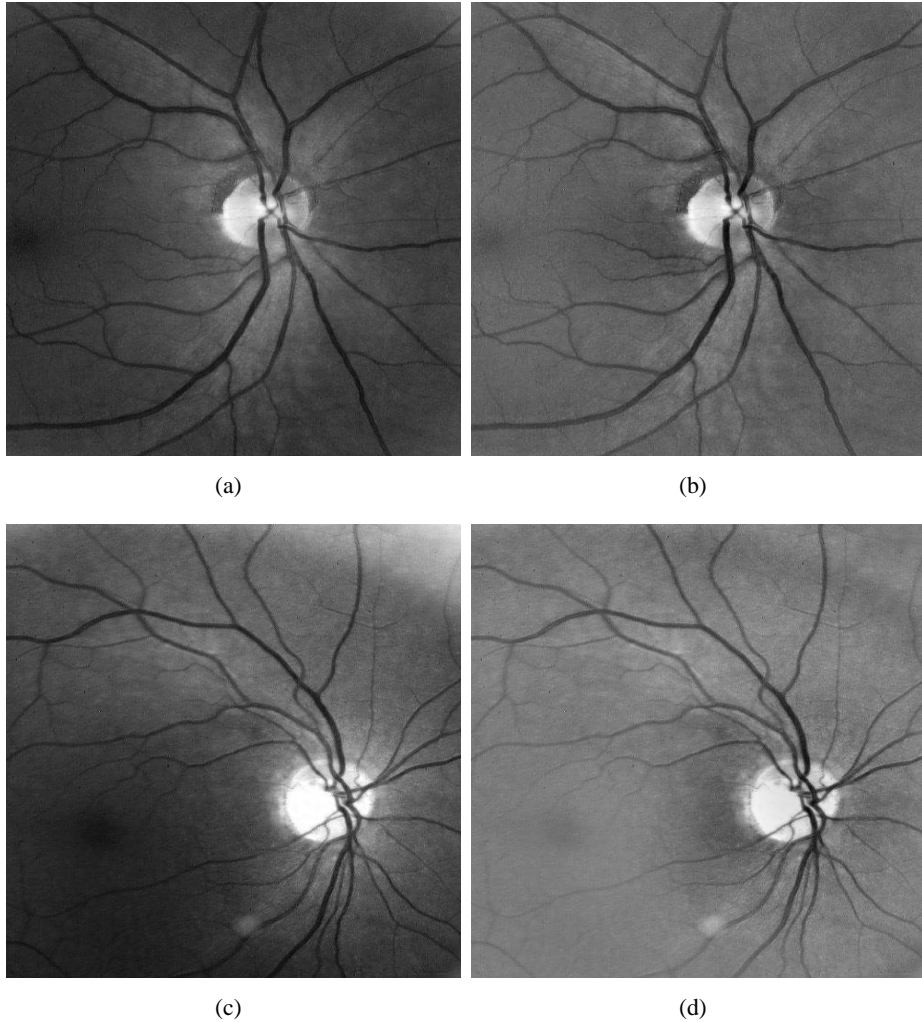


Fig. 18. a), c) Original images from the VICAVR database [21]. b) Corrected images at 5th iteration where the correlation values are (0.96, 0.84, 0.78, 0.73, 0.71) for each iteration. d) Corrected images at 5th iteration where the correlation values are (0.74, 0.68, 0.63, 0.55, 0.52) for each iteration.

V. Conclusions

The success of the method is based on the observation that if a non-uniformity is visible in an image, then the low frequency components responsible for the bias field should have a higher magnitude than other low frequency components. Our filter is automatically generated from the low frequency components of the image, which means that it belongs to the class of data-dependent filters. The results reported here clearly shows that the natural look of the image has remained intact to much of the extent after the non-uniform illumination correction which is often lost with classical filtering methods. The method is general in nature as we have tested it on five different types of images. It does not seem to require any prior knowledge of the medical imaging modality. The method only assumes that the input image is suffering from non-uniform illumination. It works fine as long as the non-uniformity is global in nature otherwise it fails. However, local illumination problems can be overcome by developing the same kind of method using wavelets, but this is beyond the scope of this manuscript.

The results demonstrate that there is a clear need of designing data-dependent filters for non-uniform illumination correction. In the future, we are planning to extend this method to volumetric data and use a more sophisticated method to convert our ideal filter to a smooth one.

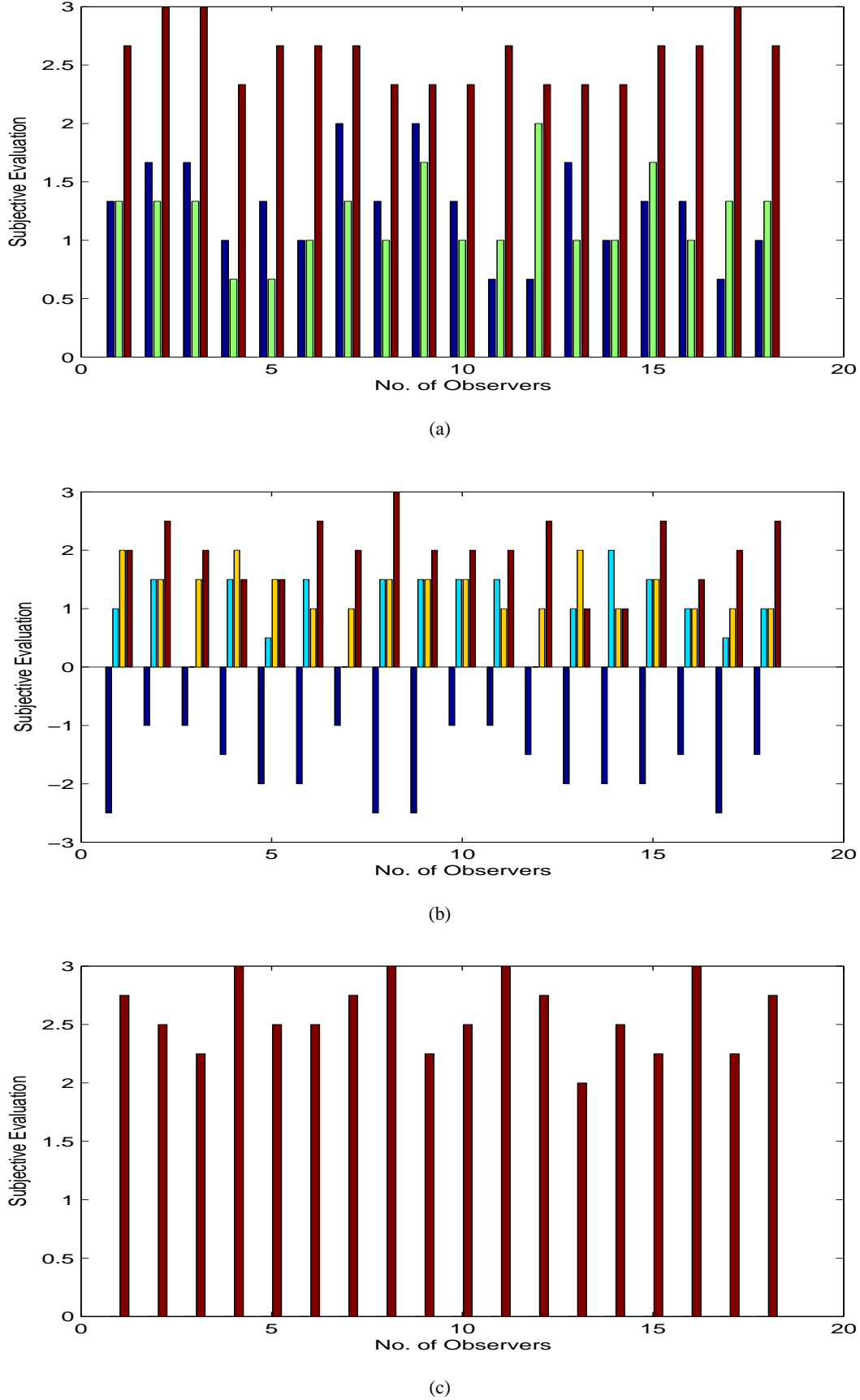


Fig. 19. a) Average subjective evaluation of the MRI images. b) Average subjective evaluation of TEM images. c) Average subjective evaluation of the retinal images after applying the proposed method. It is worth mentioning that retinal images were only compared with the original images. This was done as the retinal images do not follow the sparse distribution property and the method developed in [11] is never tested on this modality.

REFERENCES

- [1] U. Vovk, F. Pernus, and B. Lika, "A review of methods for correction of intensity inhomogeneity in MRI," *IEEE Transactions on Medical Imaging*, vol. 26, pp. 405–421, March 2007.
- [2] M. Styner, C. Brechbuhler, G. Szekely, and G. Gerig, "Parametric estimate of intensity inhomogeneities applied to MRI," *IEEE Transactions on Medical Imaging*, vol. 19, pp. 153–165, March 2000.
- [3] L. Juan and O. Gwun, "A comparison of SIFT, PCA-SIFT and SURF," *International Journal of Image Processing (IJIP)*, vol. 3, no. 4, pp. 143–152, 2010.
- [4] B. Georgescu and P. Meer, "Point matching under large image deformations and illumination changes," *IEEE Transactions on Pattern Analysis and Machine Intelligence*, vol. 26, pp. 674–688, 2004.
- [5] R. C. Gonzalez and R. E. Woods, *Digital Image Processing 3rd Edition*. Prentice Hall, 2008.
- [6] T. Tasdizen, R. Whitaker, R. Marc, and B. Jones, "Non-uniform illumination correction in transmission electron microscopy," in *MICCAI Workshop on Microscopic Image Analysis with Applications in Biology*, September 2008.
- [7] Y. Zheng, M. Grossman, S. Awate, and J. Gee, "Automatic correction of intensity nonuniformity from sparseness of gradient distribution in medical images," in *Proceedings of the 12th International Conference on Medical Image Computing and Computer-Assisted Intervention: Part II*, vol. 5762, pp. 852–859, Springer-Verlag Berlin, Heidelberg, 2009.
- [8] U. Köthe, "Edge and junction detection with an improved structure tensor," in *Pattern Recognition, 25th DAGM Symposium, Magdeburg, Germany* (B. Michaelis and G. Krell, eds.), vol. 2781 of *Lecture Notes in Computer Science*, pp. 25–32, Springer, September 2003.
- [9] L. Axel, J. Costantini, and J. Listerud, "Intensity correction in surface-coil MR imaging," *American Journal of Roentgenology*, vol. 148(2), pp. 418–420, 1987.
- [10] B. H. Brinkmann, A. Manduca, and R. A. Robb, "Optimized homomorphic unsharp masking for MR grayscale inhomogeneity correction," *IEEE Transactions on Medical Imaging*, vol. 17(2), pp. 161–171, 1998.
- [11] E. Ardizzone, R. Pirrone, and O. Gambino, "Bias artifact suppression on MR volumes," *Computer Methods and Programs in Biomedicine*, vol. 92, pp. 35–53, 2008.
- [12] R. Guillemaud, "Uniformity correct ion with homomorphic filtering on region of interest," in *IEEE International Conference on Image Processing*, vol. 2, pp. 872–875, 1998.
- [13] E. Ardizzone, R. Pirrone, and O. Gambino, "Pervasive access to MRI bias artifact suppression service on a grid," *IEEE Transactions on Information Technology in Biomedicine*, vol. 13(1), pp. 87–93, 2009.
- [14] E. Ardizzone, R. Pirrone, and O. Gambino, "Fuzzy c-means segmentation on brain MR slices corrupted by RF-Inhomogeneity," in *Proceedings of the 7th International Workshop on Fuzzy Logic and Applications: Applications of Fuzzy Sets Theory*, pp. 378–384, 2007.
- [15] E. Ardizzone, R. Pirrone, and O. Gambino, "Frequency determined homomorphic unsharp masking algorithm on knee MR images," in *13th International Conference on Image Analysis and Processing*, pp. 922–929, 2005.
- [16] K. C. Strasters, A. W. M. Smeulders, and H. T. M. V. Voort, "3-d texture characterized by accessibility measurements, based on the grey weighted distance transform," *BioImaging*, vol. 2, no. 1, pp. 1–21, 1994.
- [17] J. Pawley, ed., *Handbook of Biological Confocal Microscopy, 3rd Edition*. New York: Springer, 2006.
- [18] D. J. Fleet, "Disparity from local weighted phase-correlation," in *IEEE International Conference on Systems, Man, and Cybernetics*, pp. 48–56, October 1994.
- [19] P. K. Saha, F. W. Wehrli, and B. R. Gomberg, "Fuzzy distance transform: Theory, algorithms, and applications," *Computer Vision and Image Understanding*, vol. 86(3), pp. 171–190, 2002.
- [20] J. J. Staal, M. D. Abramoff, M. Niemeijer, M. A. Viergever, and B. V. Ginneken, "Ridge based vessel segmentation in color images of the retina," *IEEE Transactions on Medical Imaging*, vol. 23, pp. 501–509, April 2004.
- [21] "VICAVER, VARPA images for the computation of the arterio/venular ratio database," <http://www.varpa.org/RetinalResearch.html> 2009.
- [22] L. Kubecka, J. Jan, and R. Kolar, "Retrospective illumination correction of retinal images," *International Journal of Biomedical Imaging*, vol. 2010, pp. 1–10, 2010.
- [23] R.-S. Kwan, A. Evans, and G. Pike, "MRI simulation-based evaluation of image-processing and classification methods," *IEEE Transactions on Medical Imaging*, vol. 18, pp. 1085–1097, Nov. 1999.
- [24] N. Otsu, "A threshold selection method from gray-level histograms," *IEEE Transactions on Systems, Man, and Cybernetics*, vol. 9, pp. 62–66, Jan. 1979.